BMP-2, PDGF-BB, and bone marrow mesenchymal cells in a macroporous -TCP scaffold for critical-size bone defect repair in rats

2015 Biomed. Mater. 10 045008

(http://iopscience.iop.org/1748-605X/10/4/045008)

Biomedical Materials

PAPER

BMP-2, PDGF-BB, and bone marrow mesenchymal cells in a macroporous β-TCP scaffold for critical-size bone defect repair in rats

RECEIVED
20 May 2015

ACCEPTED FOR PUBLICATION
5 June 2015

PUBLISHED
23 July 2015

Carlos del Rosario[1], María Rodríguez-Évora[1], Ricardo Reyes[1,2], Araceli Delgado[1,2] and Carmen Évora[1,2]

[1] Department of Chemical Engineering and Pharmaceutical Technology, University of La Laguna, 38200 La Laguna, Spain
[2] Institute of Biomedical Technologies (ITB), University of La Laguna, 38200 La Laguna, Spain

E-mail: cevora@ull.es and adelgado@ull.es

Keywords: bone morphogenetic protein-2 (BMP-2), platelet-derived growth factor (PDGF-BB), beta-tricalcium phosphate (β-TCP), mesenchymal stem cells (MSCs), robocasting, bone repair

Abstract

The aim of this work was to study the bone repair induced by bone morphogenetic protein-2 (BMP-2), rat mesenchymal stem cells (rMSCs), and platelet-derived growth factor (PDGF-BB) incorporated in a macroporous beta-tricalcium phosphate (β-TCP) system fabricated by robocasting, and to identify the most beneficial combination in a critical rat calvaria defect. BMP-2 was formulated in microspheres to provide a prolonged, local concentration, whereas PDGF-BB, which acts during the initial stage of defect repair, was incorporated in a thin layer of crosslinked alginate. Approximately 80% of PDGF-BB and 90% of BMP-2 were released into the defect during the first 2 d and 3 weeks, respectively. Histological analyses indicated a minor synergistic effect in the BMP-2-MSC groups. In contrast, significant antagonism was found with combined BMP-2 and PDGF-BB defect treatment. The high-grade repair induced by BMP-2 rules out any advantage from combining BMP-2 with PDGF-BB or MSCs, at least with this scaffold and defect model.

1. Introduction

The use of autologous or allogenic bone grafts for bone healing has drawbacks [1–3]. Bioactive systems with three main components, i.e. a scaffold, cells, and growth factors (GFs), have been proposed as an alternative strategy. Key parameters to design and fabricate functional, bioactive systems comprise the composition, pore architecture (including porosity, pore size, interconnectivity, and channel orientation) [4–7], as well as the capacity for controlling GF release [8]. However, conventional methods [8–11], such as solvent casting/particulate leaching, melt molding, and gas foaming, generally result in non-homogeneous structures with irregular pore shapes, insufficient pore interconnectivity, and poor reproducibility. By contrast, rapid prototyping (RP) techniques facilitate the elaboration of different polymer and ceramic scaffolds with varying geometries [12–16]. In particular, the direct-write assembly (robocasting) technique, applied to develop the herein studied β-tricalcium phosphate (β-TCP) system, permits obtaining structures with well-defined and reproducible architectures with improved porosity [17–20].

Pore sizes of less than 1 μm have been reported to be essential for protein interactions and, therefore, scaffold bioactivity. Pores in the range of 1–20 μm allow cellular attachment and development, and pores wider than 100 μm favor bone ingrowth and new vessel formation [21, 22]. Moreover, calcium phosphates provide Ca^{2+} as well as PO^{4-} in the fracture environment, which may promote tissue healing and new bone formation [23]. Compared to other calcium phosphates, β-TCP shows a high resorption rate and biodegradability [24]. Scaffolds are intended to substitute for the multiple functions of the lost extracellular matrix (ECM). However, despite their optimized structure, scaffolds fail to achieve the molecular complexity and organization of native tissue matrices. This flaw has led to scaffold improvement by incorporating cells and signaling molecules that, in turn, stimulate cell migration, proliferation, and differentiation, all of which are essential for tissue development, homeostasis, and repair. The implantation of such mesenchymal stem cell (MSC)-seeded, porous structures into bone defects enhances tissue formation. MSCs are capable of self-renewing and differentiating into osteoblasts [25]. Based on their role as signaling proteins in bone healing, GFs contribute greatly to render bioac-

tivity to supportive structures [26–28]. To date, only bone morphogenic protein (BMP)-2 and BMP-7 are in clinical use due to their osteoinductive capacity that promotes differentiation of MSCs into osteoblasts and ECM formation [26]. However, their short half-lives call for alternative formulations to delay their degradation and extend their active phase [29]. However, platelet-derived growth factor (PDGF) has chemotactic and mitogenic effects on osteoblast lineage cells and osteoblasts [27]. Thus, PDGF stimulates osteoblast proliferation and also differentiation. Moreover, PDGF is known for its angiogenic effect through the upregulation of vascular endothelial growth factor (VEGF) expression. Because angiogenesis is critical in skeletal development and bone fracture repair, PDGF may enhance bone regeneration not only by attracting osteoprogenitor cells and inducing their proliferation but also by stimulating angiogenesis [30].

The overall objective of this study was to investigate the local osteogenic effect of BMP-2, rMSCs, and PDGF-BB incorporated in a macroporous β-TCP scaffold designed to mimic the physiological GF delivery sequence, and to identify the combination that best regenerates an 8 mm critical-size rat calvaria bone defect. A β-TCP scaffold with a predefined, porous, radial architecture was elaborated by robocasting, subsequently loaded with BMP-2, incorporated in microspheres of PLGA 75:25 as a sustained-release formulation, rMSCs (rat MSCs), or both, and evaluated in terms of bone healing. In addition, the impact of the *in vitro* culture period was studied by comparing 3 week rMSCs with overnight cultures. Alternatively to the rMSCs, two distinct doses of PDGF-BB and their combination with BMP-2 in microspheres of PLGA 50:50 were evaluated. The PDGF-BB was incorporated in a thin layer of crosslinked alginate, which surrounded the scaffold for fast release.

Although calcium phosphates are widely used in bone tissue engineering, the literature presents only few studies on RP of scaffolds that support a physiological bone regeneration process. In this study, both cells and GFs have been incorporated into a scaffold fabricated by robocasting. This scaffold provides controlled porosity to enhance MSC differentiation into osteoblast. Beyond that, the release rate of the two GFs was controlled to imitate the physiological sequence. PDGF-BB was included in an alginate film to make it available for the initial step of the healing process. In contrast, BMP-2 was formulated in microspheres for prolonged release, as it acts throughout the whole regeneration period.

According to the literature, this may be the first study regarding a scaffold produced by robocasting and loaded with a combination of cells and GFs that is evaluated both *in vitro* and *in vivo*.

2. Materials and methods

2.1. System preparation

Robocast β-TCP scaffolds were purchased from and made by Ceramics 3D LLC (Badajoz, Spain), according to our specifications. A fabrication process described in the literature was applied [17, 18, 31, 32]. Briefly, a robotic device was used to deposit layers of slurry to form a mesh of ceramic rods via direct-write assembly. According to the reports of the manufacturer [17, 18, 31, 32], the procedure consists of depositing the slurry (a stable suspension of calcium phosphate particles) via a printing syringe into an oil bath. Subsequently, the scaffolds are sintered at a pre-established temperature.

The cylindrical scaffolds with an external diameter of 8 mm and a central, round hole 3 mm in diameter consisted of the described layers of β-TCP rods (84 wt% β-TCP and 16 wt% α-CPP [α-calcium pyrophosphate]) in alternating concentric versus radial patterns, which led to highly regular macroporosity. The central scaffold hole was filled with a cylindrical tablet of microspheres.

BMP-2 (Biomedal Life Sciences, Sevilla, Spain) containing microspheres of either PLGA 75:25 (Resomer® RG755S, Evonik, Germany) or PLGA 50:50 (Resomer® RG504, Evonik, Germany) were prepared by the double emulsion method as previously described [33]. Briefly, 180 μg of rhBMP-2 in 200 μL of 0.07% polyvinyl alcohol (PVA) were vortexed with 2 mL of a PLGA methylene chloride solution (50 mg mL^{-1}). Then, the emulsion was poured into a 0.1% PVA (w/v) solution to evaporate the organic solvent. Microspheres were collected by filtration and lyophilized. The tablets were fabricated by compressing a variable quantity of microspheres (depending on the encapsulation efficiency) that contained an effective amount of 6 μg of BMP-2, complete with 15 mg with blank microspheres, at 37.5 MPa for 2 min using a Carver hydraulic press.

The scaffolds were coated with a thin layer of alginate according to their experimental application (table 1). Thus, the scaffolds were immersed for 20 min in an alginate solution (1.5% w/v) and the alginate was subsequently crosslinked with $CaCl_2$ (0.75% w/v). Then, $CaCl_2$ remains were removed in three wash steps of 10 min each and the scaffolds were freeze-dried. A few minutes before implantation, the tablet was introduced into the central hole and 250 ng or 500 ng of PDGF-BB in a 12 μL solution (acetic acid 20 mM and BSA 0.1%) was dropped in aliquots of 1.5 μL onto each of the eight sections of the external structure (figure 1(a)).

β-TCP scaffolds filled with a tablet of microspheres prepared with PLGA 75:25 were designated P-scaffolds. Scaffolds coated with alginate and filled with a tablet of microspheres of PLGA 50:50 were named AP-scaffolds.

2.2. System characterization

Microsphere size was assessed with a particle size analyzer (Mastersizer 2000; Malvern Instruments). Several batches of microspheres with BMP-2 were prepared using ^{125}I-BMP-2 to determine encapsulation efficiency and to perform the *in vivo* release assays. BMP-2 was labeled with ^{125}I according to the iodogen method [34]. Briefly, 25 μL of BMP-2 (1 mg mL^{-1}) and

Table 1. Experimental groups (9 rats each).

Group	Comments
C	Control group: empty defect
P-B[a]	Blank group: blank system
P-BMP[a,b]	System with 6 μg BMP-2 in microspheres
P-MSC-O/N	System seeded with 200 000 cells, cultured overnight
P-MSC-3w	System seeded with 200 000 cells, cultured for 3 weeks
P-BMP-MSC-O/N	System seeded with 200 000 cells, cultured overnight, and 6 μg BMP-2 in microspheres
P-BMP-MSC-3w	System seeded with 200 000 cells, cultured for 3 weeks, and 6 μg BMP-2 in microspheres
AP-B[a]	Blank group: blank system
AP-BMP[a,b]	System with 6 μg BMP-2 in microspheres
AP-MSC-O/N	System seeded with 200 000 cells, cultured overnight
AP-BMP-MSC-O/N	System seeded with 200 000 cells, cultured overnight, and 6 μg BMP-2 in microspheres
AP-PDGF-250[b]	System with 250 ng PDGF-BB in the alginate layer
AP-PDGF-500	System with 500 ng PDGF-BB in the alginate layer
AP-BMP-PDGF-250	System with 250 ng PDGF-BB in the alginate layer and 6 μg BMP-2 in microspheres
AP-BMP-PDGF-500	System with 500 ng PDGF-BB in the alginate layer and 6 μg BMP-2 in microspheres

[a] Including 3 additional animals for *in vivo* system characterization.
[b] Including 5 additional animals for *in vivo* release assays.

10 μL of ^{125}INa (1 mCi) (Perkin-Elmer, Boston, MA), adjusted to 100 μL with 0.5 M phosphate buffer, pH 7.0, were placed in a Pierce® pre-coated iodination tube (Thermo Scientific, Rockford, IL). After 15 min of incubation at room temperature and 120 rpm, 100 μL of saturated tyrosine solution in PBS was added to eliminate the unreacted ^{125}I. Purification of the reaction mixture was performed using a Zeba™ Spin Desalting Column (Thermo Scientific) following the manufacturer's instructions. ^{125}I-BMP-2 labeling yield and radiolabeling stability were checked by thin layer chromatography as described previously [35].

^{125}I-PDGF-BB (Perkin-Elmer) was used to determine the incorporation efficiency of the PDGF-BB in the alginate film and to perform the *in vivo* release assay.

The specific surface area (BET area) of the external phosphate structure of the P-scaffolds and AP-scaffolds was assessed by nitrogen adsorption (Gemini; Micromeritics, Norcross, GA).

Porosity (P) of the external phosphate and the tablet of microspheres were calculated separately using the gravimetric method and equation (1):

$$P(\%) = \left(1 - \frac{\rho_{app}}{\rho_{true}}\right) \times 100 \qquad (1)$$

where ρ_{app} and ρ_{true} are the apparent and real densities of the scaffolds or tablets, respectively. The ρ_{app} of each scaffold or tablet equals its total mass divided by its total volume. The ρ_{true} was assessed by means of a helium pycnometer (AccuPyc 1330 Pycnometer; Micromeritics). Tablet porosity was also determined by mercury intrusion porosimetry (Autopore IV 9510 Porosimeter; Micromeritics).

Morphology of the assembled system was observed by stereo microscopy (Leica M205 C, Leica LAS, v.3 software) and scanning electron microscopy (SEM; Jeol JSM-6300). Atomic force microscopy (AFM) operating in tapping mode (Nanoscope IIIa; Digital Instruments Veeco, Santa Barbara, CA) was used to scan the β-TCP surface and grain size distribution.

2.3. Cells: rat bone marrow stem cell isolation

Bone marrow rMSCs were obtained from femur and tibiae bone marrow of 6 week-old male Sprague-Dawley rats as described [36]. Whole bone marrow was pooled and resuspended in Dulbecco's minimal essential medium with 4.5 g L^{-1} glucose, 20% fetal bovine serum (FBS), 50 UI mL^{-1} penicillin, 50 μg mL^{-1} streptomycin, and 200 mM stabilized L-glutamine, seeded on cell culture plastic, and incubated at 37 °C and 5% CO_2. Cells were detached when confluent and were frozen for later experimental use.

2.3.1. Cell seeding

Scaffolds were sterilized with UV light on both sides for 30 min each and subsequently immersed for 5 min in PBS to favor scaffold wettability. Thereafter, scaffolds were placed in 48-well culture plates, seeded with 2 × 10^5 rMSCs, and incubated for 2 h at 5% CO_2 and 37 °C for cell attachment. Then, 1.5 mL of fresh culture medium was added. Medium was changed every 3 to 4 d. According to the experimental groups (table 1), cells were cultivated either overnight (O/N) or for 3 weeks before implantation. After a rinse step with PBS, scaffold-adhered cells were quantified by the metabolic reduction of XTT (2,3-bis(2-methoxy-4-nitro-5-sulfophenyl)-5-[(phenylamino)carbonyl)]-2H-tetrazolium hydroxide) (XTT colorimetric assay; Roche, Madrid, Spain) at 492 nm (reference 690 nm).

To visualize viable cells, scaffolds were incubated for 30 min in 500 μL of 1 μg mL^{-1} calcein AM (Fluka; Sigma-Aldrich, Madrid, Spain) in PBS. After a wash

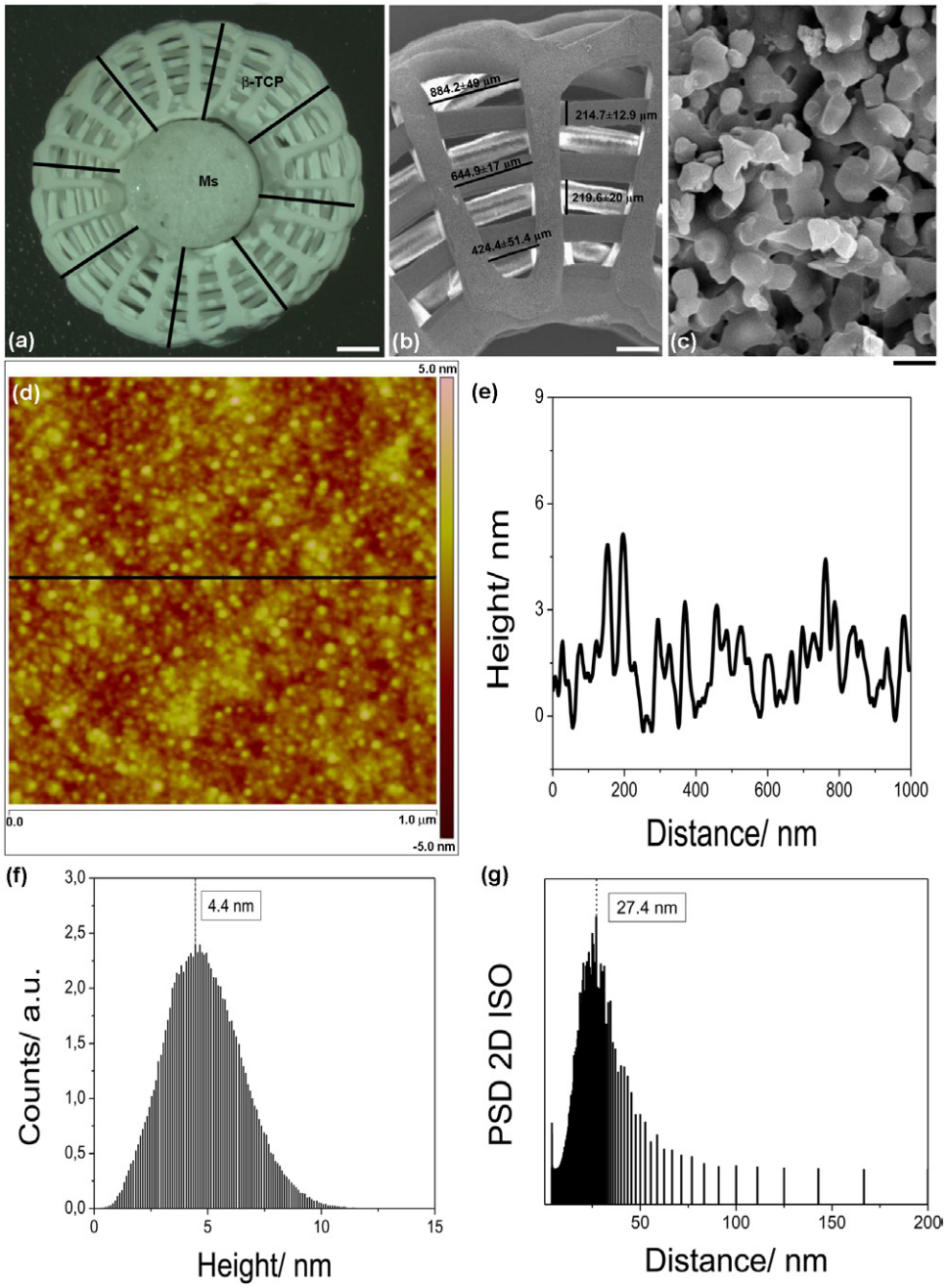

Figure 1. β-TCP scaffold characteristics. (a) Stereo microscope images of the β-TCP scaffold indicating the eight sections where the PDGF-BB droplets were placed. (b), (c) SEM images of the macropores and micropores of the external β-TCP structure. (d)–(g) Parameters and image obtained by AFM: (d) nanoporosity; (e), (f) β-TCP grain height; and (g) intergrain distance. Scale bars: (a) = 1 mm; (b) = 400 μm; (c) = 10 μm.

step, cells were observed with a Zeiss (Jena, Germany) Axiovert 40 CFL inverted microscope and photomicrographs were taken with a Canon (Tokyo, Japan) PowerShot A620 digital camera.

2.4. Flow cytometry analysis

rMSCs were cultured on P-scaffolds and AP-scaffolds in triplicate as described above. At each sampling time point, cells were detached with 0.5 mL of trypsine for 8 min at 37 °C. Then, the cells were incubated at 4 °C for 30 min with FITC mouse anti-rat CD45™ (BD Pharmingen), PE mouse anti-Rat CD90/Mouse CD90.1™ (BD Pharmingen), and V450 hamster anti-rat CD29™ (BD Horizon) antibodies. Subsequently, cells were washed three times with 200 μL of PBS each and centrifuged at 4 °C for 8 min at 300 *g*. Every system was analyzed in triplicate with a Miltenyi Biotec flow cytometer (Macsquant Analyser, Germany). An aliquot of rMSCs from culture plastic (2D culture) was analyzed as a control to scaffold-seeded cells.

2.5. Animal experiments

Male Sprague-Dawley rats weighing 250–300 g were used in this study. All experiments were previously

approved by the Ethics Committee for Animal Care of the University of La Laguna and were performed in conformity with the EC directive on Care and Use of Animals in Experimental Procedures (2010/63/UE). Experimental groups are detailed in table 1.

2.5.1. Surgical procedure

Surgical procedures were performed under aseptic conditions as previously described [8]. A standardized, critical, circular, transosseous defect of 8 mm in diameter [37] was set in the crania of anesthetized rats (ketamine 100 mg kg^{-1} and xylazine 10 mg kg^{-1}). First, buprenorphine (0.05 mg kg^{-1}) was administered subcutaneously (SC) to reduce postsurgical pain. Once the calvaria bone was exposed, the defect was created with a bone trephine bur under continuous saline buffer irrigation. Then, the scaffold was inserted, the skin was stapled, and 1 mL of saline solution was injected SC to restore blood volume. Atipamezol (1 mg kg^{-1}) was administered SC to reverse the anesthesia, and 12 h and 36 h later SC injections of buprenorphine were administered.

2.5.2. In vivo release assay: ^{125}I-BMP-2 and ^{125}I-PDGF-BB

^{125}I-BMP-2 and ^{125}I-PDGF-BB release kinetics were monitored periodically by measuring the remains at the calvaria defect using an external gamma counter (Captus®; Nuclear Iberica) as previously described and validated [38]. Briefly, the detector was placed onto the defect site of sedated rats (Ketamine 75–100 mg kg^{-1}) and the remaining radioactivity was measured at 27 keV. Reading at time point 0 was considered the given dose (100%).

2.5.3. Scaffold evolution in vivo

A total of 12 rats were used to study the evolution of the scaffold material after implantation. After 4 weeks, three rats of each of the AP-B and AP-BMP groups were sacrificed and the scaffolds were extracted. Similarly, after 12 weeks, the scaffolds of three rats in each of the P-B and the P-BMP groups were recovered. The scaffolds were washed with Milli-Q water, the central tablet was isolated, and both components were freeze-dried. Gel permeation chromatography was used to determine the weight-average molecular weights (Mw) and polydispersity (pd) of the polymers. A Waters® chromatograph equipped with a pump (Model 510), Rheodyne injector, differential refraction index detector (Model 410), and three columns (Styragel® HR4, HR3, and HR1) was applied at 31 °C for data acquisition using Waters Breeze software. Polystyrene monodisperse standards (Tokyo Soda) were used as references.

The empty phosphate external structure was analyzed before and after implantation by x-ray diffraction (XRD) (Phillips X'pert automated diffractometer using Cu Kα radiation at $\lambda = 1.5418$ Å) and compared to native bone pattern.

2.5.4. Histology, immunohistochemical and histomorphometrical evaluation

To determine the bone-regenerative effect of the released rhBMP-2, PDGF-BB, scaffolds seeded with rMSCs, as well as their combinations, 15 groups of 9 rats each were examined at 4, 8, and 12 weeks post-implantation (table 1).

Samples were fixed (10% formalin solution) and decalcified in Histofix® Decalcifier (Panreac, Barcelona, Spain) and prepared for histological analysis as previously described [39]. New bone formation was identified by hematoxylin-erythrosin staining. The degree of new bone mineralization was assessed with VOF trichrome stain, for which red and brown staining indicates advanced mineralization, whereas less mineralized, newly formed bone stains blue [40]. Sections were analyzed by light microscopy (LEICA DM 4000B). Computer-based image analysis software (Leica Q-win V3 Pro-image Analysis System, Barcelona, Spain) was used to histomorphometrically evaluate all sections per specimen. A region of interest (ROI) for quantitative evaluation of new bone formation was defined as the area of the tissue within the defect. The ROI consisted of a circular region of 50 mm^2, the center of which coincided with that of the defect site. New bone formation was expressed as a percentage of repair by applying equation (2)

$$\%\ \text{repair} = \frac{\text{new bone area}}{\text{original defect area within the ROI}} \times 100. \quad (2)$$

Neovascularization was quantified to determine blood vessel density and vessel surface area within the ROI. For this purpose, sections were immunolabeled with an anti-von Willebrand factor polyclonal antiserum (1/50) (DAKO, Barcelona, Spain) as described [39]. Reaction specificity was confirmed by replacing the specific antiserum with normal serum. Blood vessel density was expressed in absolute values and vessel surface area in mm^2 based on the quantitative evaluation of the ROI.

Statistical analysis was performed with SPSS.19 software. We compared the distinct treatments at every individual time point (4, 8 and 12 weeks) using the non-parametric Mann–Whitney *U*-test. Significance was set at $p < 0.05$. Results are expressed as means ± SD.

3. Results

3.1. System characteristics

Size, weight, specific surface area (BET area), and porosity of the external empty phosphate structure and the central microsphere tablet are detailed in table 2.

The mean volume diameter of the PLGA 75:25 microspheres was 182.7 μm. BMP-2 encapsulation efficiency was 78.1 ± 9%. The PLGA 50:50 microspheres showed similar values; the mean diameter was 191.1 μm and the encapsulation efficiency was 71.4 ± 5.8%. The incorporation efficiency of the PDGF-BB in the alginate film was 95.4 ± 6.0%.

Table 2. Morphological and physical scaffold parameters.

	External structure P-scaffold	External structure AP-scaffold	Internal 75:25 tablet P-scaffold	Internal 50:50 tablet AP-scaffold
Porosity (%) (gravimetric method)	77.27 ± 0.02	76.55 ± 0.02	28.35 ± 0.02	20.95 ± 0.02
Porosity (%) (mercury porosimetry)	—	—	23.6	21.6
BET area ($m^2 g^{-1}$)	0.95 ± 0.03	1.04 ± 0.03	—	—
Total pore volume of pores < 140 nm ($mm^3 g^{-1}$)	1.32	1.47	—	—
Weight (mg)	44.59 ± 4.82	46.70 ± 0.53	14.6 ± 0.25	14.6 ± 0.5
Diameter (mm)	7.94 ± 0.17	7.94 ± 0.17	3.05 ± 0.01	3.05 ± 0.01
Internal hole (mm)	3.10 ± 0.05	3.10 ± 0.05	—	—
Height (mm)	1.56 ± 0.11	1.56 ± 0.11	2.03 ± 0.05	1.88 ± 0.08

Scaffold macroporosity was visible to the naked eye and is reflected in figure 1(b). Microporosity and nanoporosity were detected by SEM (figure 1(c)) and AFM (figure 1(d)), respectively. The height of the β-TCP grains was 4.4 nm and the intergrain distance was 27.4 nm (figures 1(e)–(g))). The contribution of pores smaller than 140 nm to the porosity was determined by nitrogen adsorption and is given in table 2.

3.2. Cell culture

Compared to the 2×10^5 initially seeded cells, cell numbers on the external β-TCP structure were $5 \times 10^4 \pm 1.0 \times 10^4$ after O/N incubation, $2.8 \times 10^5 \pm 0.2 \times 10^5$ after 3 weeks of culture, and $7 \times 10^4 \pm 0.6 \times 10^4$ after O/N incubation of the alginate film-coated scaffold. Calcein AM staining revealed cell adhesion after O/N incubation (figure 2(a)). After 3 weeks, the macropores were completely filled with cells, and cellular bridge formation between the scaffold bars was clearly observable (figure 2(b)).

3.3. Flow cytometry

Flow cytometry analysis demonstrated that rMSCs were mainly positive for CD90 and CD29 and negative for CD45 as expected [41]. According to the data obtained for these surface markers, rMSCs conserve their monolayer phenotype in 3D conditions, regardless of their time in culture and the type of scaffold (figure 2(c)).

3.4. *In vivo* GF release assay

GF release from the implants was assessed at the defect site by monitoring the remaining ^{125}I-BMP-2 of the P-scaffolds and AP-scaffolds and the ^{125}I-PDGF-BB of the AP-scaffolds. We detected no difference between the ^{125}I-BMP-2 profiles of either type of scaffold (figure 3). During the initial 24 h, approximately 1.8 μg of BMP-2 was released. After 3 weeks, almost the total amount of BMP-2 had been delivered at a rate of approximately 200 ng d^{-1}. In contrast, the PDGF-BB adsorbed to the crosslinked alginate was released rapidly, whereby 83% was released during the first 2 d. Thereafter, the release rate declined and the PDGF-BB was completely released within approximately 2 weeks (figure 3).

3.5. *In vivo* system degradation

The Mw of the remaining PLGA 75:25 (60 kDa) microspheres at the defect site decreased to approximately 16 kDa over the course of 12 weeks (figure 3). In contrast, the resulting Mw of the PLGA 50:50 (50 kDa) microspheres was approximately 8.7 kDa after 4 weeks (figure 3). Thereafter, it was no longer possible to collect PLGA 50:50 microspheres. In contrast, the β-TCP scaffold conserved its chemical composition. XRD patterns showed that the peak height ratios between 27.8 and 31.07 and between 31.07 and 34.44 did not change with time. However, in samples of the P-BMP group an increase of background in the range of 30.85–35.17 was detected at 12 weeks, which coincided with a broad peak observed in the native bone sample (figure 4). These data support bone tissue formation within the β-TCP scaffold.

3.6. Histological and histomorphometrical evaluation

3.6.1. Histological evaluation

No or little tissue formation was observed in the control (C) and blank (P-B and AP-B) groups (figures 5(a)–(f)) throughout the experimental period.

Four weeks post-implantation, there was a slight increase in the degree of repair in the P-BMP group (figure 6(a)), AP-BMP group (figure 6(b)), and their combinations with rMSCs (P-BMP-MSC-O/N;, figure 6(c); P-BMP-MSC-3w, figure 6(e); AP-BMP-MSC-O/N, figure 6(d)) compared to the rest of the experimental groups. Mineralized, newly formed bone was observed both in the phosphate zone of the scaffold and in the central area (figures 6(d) and (e)). Detailed analysis revealed that much space was occupied by bone marrow (figure 6(f)). Furthermore, immature bone containing abundant preosteoblast-like cells was observed (figure 6(g)). However, a poor repair response was found in most of the experimental groups with rMSCs (figure 7(a)), PDGF-BB (figure 7(b)), and PDGF-BB combined with BMP (figure 7(c)). The modest quantity of newly formed bone was poorly mineralized and located on the peripheral area of the defect (figures 7(a)–(c)).

Eight weeks post-implantation, the AP-PDGF-250 (figure 8(a)), AP-PDGF-500 (figure 8(c)), and AP-MSC-O/N (figure 8(e)) groups, as well as P-MSC-O/N (figure

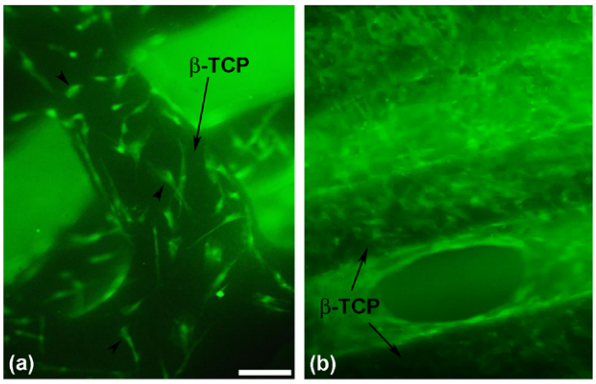

(c)

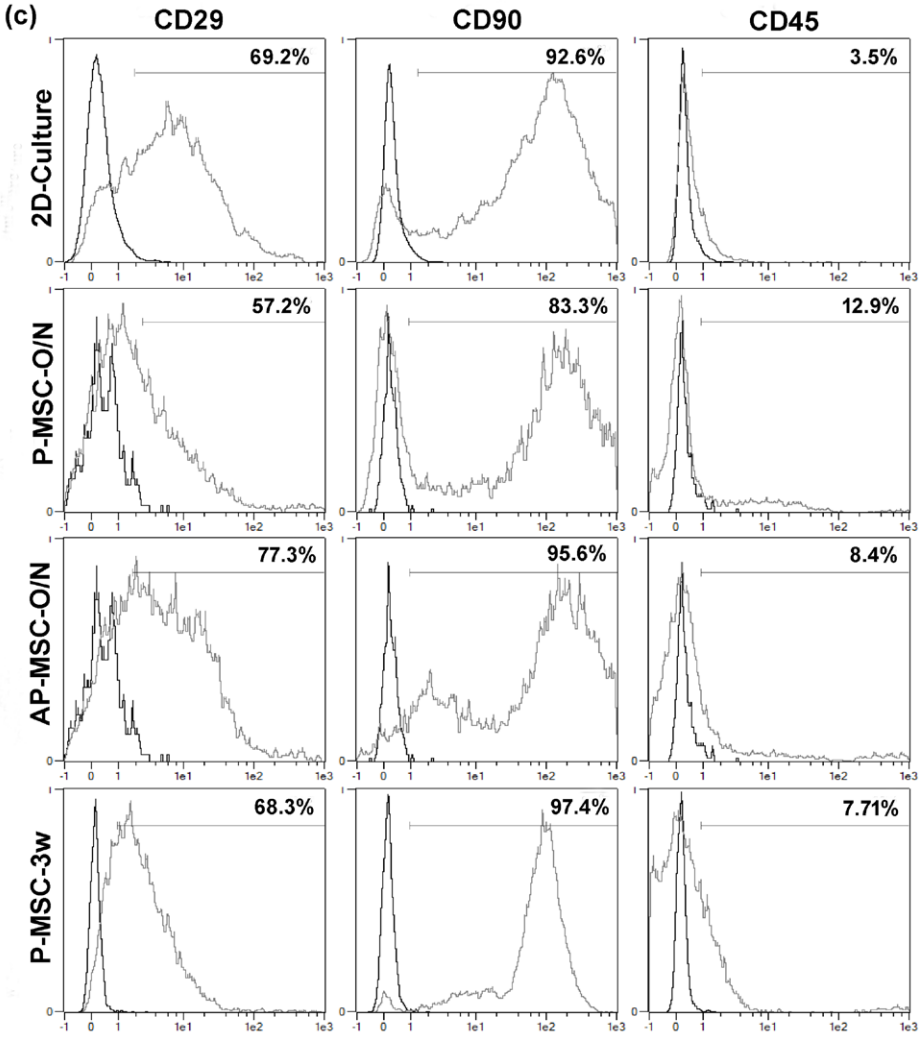

(d)

	CD 29	CD 90	CD 45
2D-Culture	67.12±2.09%	91.19±1.53%	3.17±0.25%
P-MSC-O/N	59.70±4.95%	90.60±8.36%	10.47±3.98%
AP-MSC-O/N	78.96±1.50%	94.83±1.18%	9.58±1.49%
P-MSC-3w	75.60±9.53%	92.32±4.46%	5.60±1.83%

Figure 2. Representative fluorescence photomicrographs of calcein-stained rMSCs in P-scaffolds after overnight incubation (a) and 3 weeks of culture (b). Representative flow cytometry analysis of cell-surface markers in rMSCs cultured in plate (2D-culture), in the P-scaffold overnight (P-MSC-O/N), in the AP-scaffold overnight (AP-MSC-O/N), and in the P-scaffold for 3 weeks (P-MSC-3w) (c). The mean percentage of all cells from three independent experiments is shown in the table (d). Scale bars: (a), (b) = 50 μm.

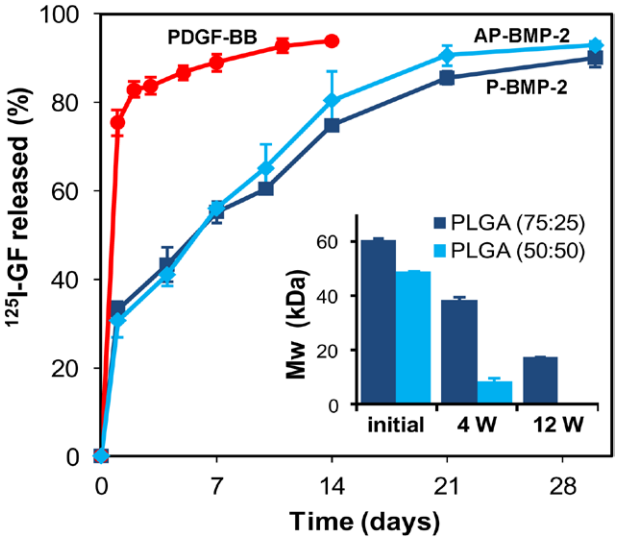

Figure 3. Cumulative PDGF-BB and BMP-2 release profiles after implantation of the AP-scaffolds and P-scaffolds ($n = 5$). Inset: progression of the weight-average molecular weight (Mw) of PLGA microspheres incorporated in AP-scaffolds and P-scaffolds implanted in an 8 mm rat bone defect ($n = 3$).

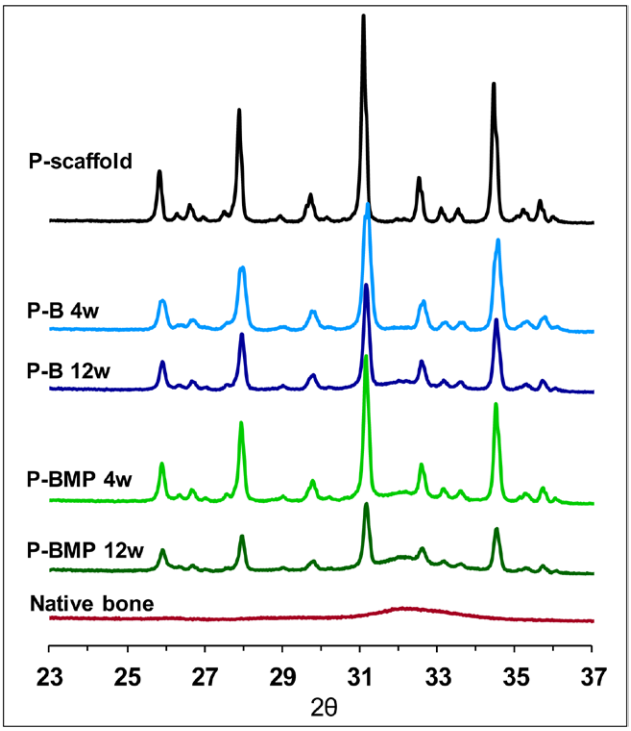

Figure 4. Comparison of the XDR pattern of the native calvaria bone with the patterns of P-scaffolds before implantation and after extraction from the P-B and the P-BMP experimental group 4 and 12 weeks post-implantation.

8(b)) and P-MSC-3w (figure 8(d)) groups, showed a slight increase in their repair responses at 4 weeks. Conversely, all groups with BMP-2 (figures 9(a) and (b)) and their combinations (figures 9(c)–(f)) had a significantly enhanced repair response at 4 weeks. In addition, immature bone was observed in the areas surrounding the newly formed bone tissue. In the P-scaffold groups, many PLGA 75:25 microspheres were still detectable in the central defect area (figures 9(a), (c) and (e)).

At 12 weeks, while the blank defects remained unchanged compared to those at 8 weeks (figures 5(e) and (f)), the P-MSC-O/N (figure 10(a)) and P-MSC-3w (figure 10(c)) groups showed a slight increase in bone formation. In the AP-MSC-O/N group, the increase in repair from weeks 8 to 12 was negligible (figure 10(c)). The groups treated with BMP-2 and their combinations with cells (P-BMP, figure 11(a); P-BMP-MSC-O/N, figure 11(c); P-BMP-MSC-3w, figure 11(e); AP-BMP, figure 11(b); AP-BMP-MSC-O/N, figure 11(d)) exhibited an important increase in bone formation. The repair in the BMP-MSC group was to some extent more evident than that in the

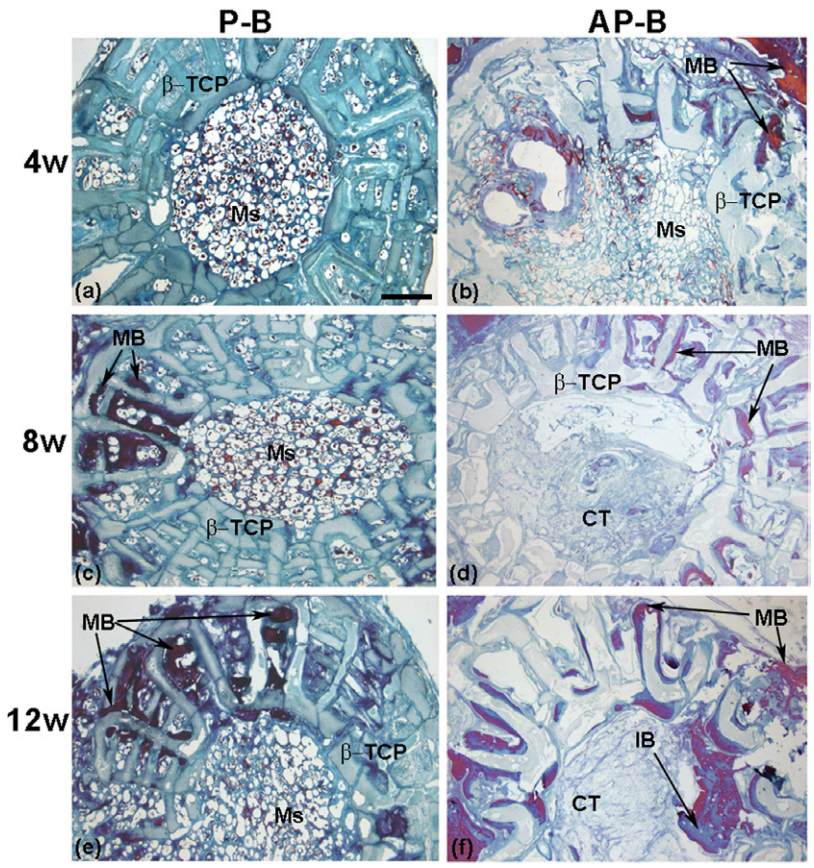

Figure 5. Representative photomicrographs of horizontal sections of calvaria defects in rats in the experimental groups P-B and AP-B at 4 (a), (b), 8 (c), (d), and 12 (e), (f) weeks post-implantation showing little or no defect repair. The scaffold structure (a)–(f) as well as the microspheres in one of the systems (a), (c), (e) were evident at all three time points. CT: connective tissue; β-TCP: beta-tricalcium phosphate; Ms: microspheres; IB: immature bone; MB: mineralized bone. Scale bar = 1 mm.

BMP-2 group. However, after 8 weeks, the AP-scaffolds loaded with BMP-2 and either of the two doses of PDGF-BB (AP-BMP-PDGF-250, figure 11(f); AP-BMP-PDGF-500, not shown) had generated similar responses as observed in the AP-BMP and AP-BMP-MSC-O/N groups (figures 11 (b) and (d)).

However, the degree of repair in groups AP-BMP-PDGF-250 (figure 11(f)) and AP-BMP-PDGF-500 was substantially lower than in groups AP-BMP and AP-BMP-MSC-O/N at 12 weeks (figures 11(b) and (d)). Hence, the repair response with BMP-2 was lower when combined with PDGF-BB than when applying BMP solely (AP-BMP). In the groups with the low repair response, the mineralized, newly formed bone was only observed in the defect periphery, the outer zone of the scaffolds, 8 and 12 weeks post-implantation. On the contrary, defect areas of the groups with high-grade repair were almost healed. The β-TCP scaffolds (P-scaffolds and AP-scaffolds) remained in the implantation zone. No signs of scaffold fragment phagocytosis were detected, although fragmentation and erosion were observed in different zones of the phosphate structure (figures 5–11). New bone filled virtually all available space between the bars and covering all scaffold surfaces, with the growing bone in intimate contact with the phosphate structure (figure 11(g)) and the central zone almost completely filled. Although some PLGA 75:25 microspheres still remained in the central area (figure 11(g)), they were covered by growing bone, which filled the spaces in between. In contrast, remnants of PLGA 50:50 microspheres were observed only 4 weeks post-implantation (figure 11(h)). Detailed analysis revealed absence or only minor presence of immature bone. In addition, normally distributed bone marrow was observed between the bone trabeculae.

The analysis of transversal sections from animals euthanized 12 weeks post-implantation showed little or no bone formation in groups P-B and AP-B (figures 12(a) and (b)). There was newly formed bone throughout the defect area in the groups with BMP-2 holding scaffolds as well as groups BMP-MSC and BMP-PDGF-BB (figures 12(c)–(f)). Mineralization in newly formed bone was similar to that in host bone. In rats implanted with P-scaffolds, bone thickness in the defect area was greater than in the host bone, although much of the space was occupied by the microspheres and the β-TCP structure (figure 12(c)). However, bone thickness in defects implanted with PA-scaffolds was similar to that in the host bone (figures 12(d)–(f)). Bone structure also resembled that of the host bone with both types of scaffolds. Bone trabeculae were observed around the β-TCP fragments and the 75:25 microspheres in P-scaffolds (figure 12(g)), and bone marrow was observed in the fragment area of the AP-scaffolds (figure 12(h)).

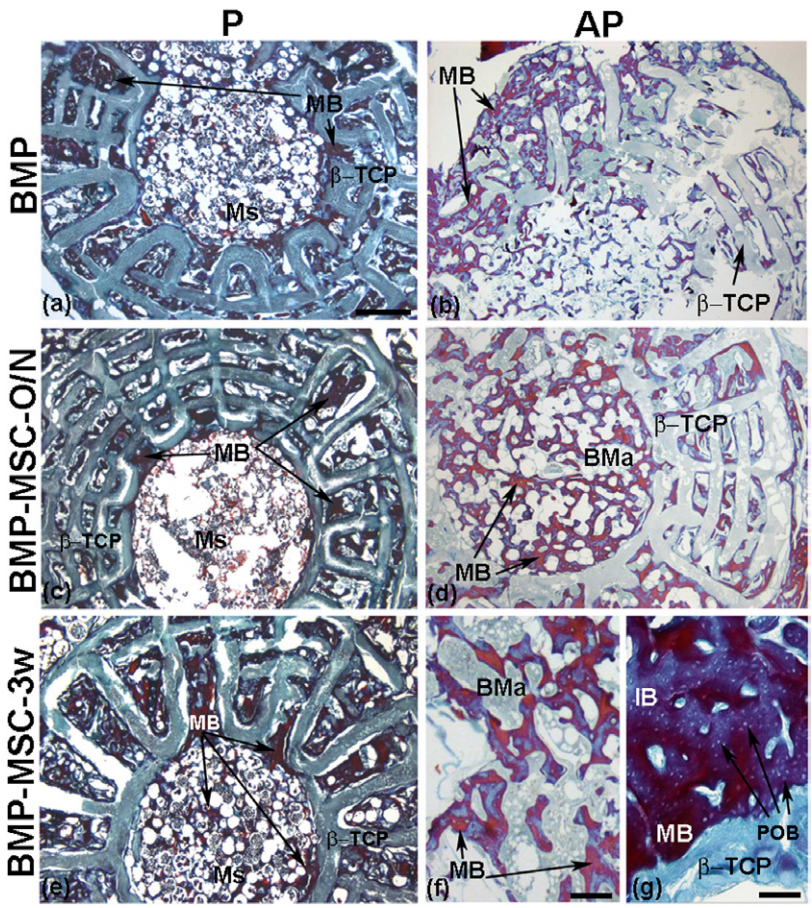

Figure 6. Representative photomicrographs of horizontal sections of calvaria defects in rats in the experimental groups P-BMP (a), AP-BMP (c), P-BMP-MSC-O/N (b), AP-BMP-MSC-O/N (d), and P-BMP-MSC-3w (e) showing differential degrees of repair 4 weeks post-implantation. (f), (g) Details at high magnification illustrate newly formed bone and bone marrow in the defect center (f) and within the newly formed bone mineralized bone (red), and areas of immature bone (blue) with numerous preosteoblastic cells (g). β-TCP: beta-tricalcium phosphate; Ms: microspheres; IB: immature bone; MB: mineralized bone; BMa: bone marrow; POB: preosteoblastic cells. Scale bars = 1 mm (a)–(e), 200 μm (f), 100 μm (g).

3.6.2. Histomorphometrical evaluation

At 4 weeks post-implantation, histomorphometrical analysis confirmed defect repair ranging from 10% to 25% of the total area with significant differences between both BMP-2 and its combinations with rMSCs with respect to the rest of the groups (figure 13).

Eight weeks post-implantation, repair was less than 20% in the control and blank groups as well as in the groups treated with PDGF-BB or rMSCs (both O/N and 3 weeks), with no significant difference between them (figure 13). The groups treated with BMP-2 or BMP-2 combined with either PDGF-BB or rMSCs exhibited defect repair of approximately 40%, representing a significant difference compared to the other groups (figure 13).

Compared to 8 weeks post-implantation, the situation had not changed much after 12 weeks; grades of repair in the control and blank groups (P-B and AP-B) and groups AP-MSC-ON, AP-PDGF-250, and AP-PDGF-500 were similar to those before then (figure 13). However, defect repair with rMSC seeded P-scaffolds gave rise to rates of approximately 40%, with significant difference compared to both the control and blank groups (figure 13). Groups treated with BMP-2 or its combination with rMSCs further increased their repair rates (figure 13). Particularly, P-scaffolds loaded with BMP-2 alone or in combination with rMSCs showed defect repair of approximately 80%.

The vascularizing effect of PDGF-BB was studied in the AP-scaffold. There was a moderate increase in blood vessel density in the groups treated with PDGF-BB or BMP-2 combined with PDGF-BB at either dose throughout the whole experimental period. Particularly at 8 weeks post-implantation, differences in blood vessel density were significant compared to the control and blank groups (figure 14(a)). There were no significant differences in vessel surface areas within the PDGF-BB treated groups at any time point (figure 14(b)). Although the data suggested a tendency for increased vessel formation between 4 and 8 weeks in the groups treated with PDGF-BB and its combinations, this did not seem to have any effect on the defect repair rate.

4. Discussion

In this study, the robocasting method was used to fabricate highly regular, macroporous β-TCP scaffolds

for bone repair characterized by decreasing pore sizes toward the internal zone.

MSC differentiation and proliferation of preosteoblastic cells have been reported to be highly susceptible by the pore geometry of a scaffold [42]. The thin bars as well as the microporosity and nanoporosity contributed to the increased specific surface area of the β-TCP scaffolds and enhanced the contact area between the material and the biological environment. In fact, enhancement of cell interaction due to nanotopography has been reported in previous works [43]. Perhaps as a consequence, there was substantial cell viability on the β-TCP scaffold material; rMSCs attached, spread, and proliferated well on the scaffold surfaces. After 12 h, calcein AM fluorescence images showed fully spread cells and relatively few round cells on the O/N scaffolds. Cell survival in 3D constructs is limited by oxygen and nutrient supply. However, the highly porous and interconnected structure of the scaffolds fabricated by robocasting favored cell adhesion and survival. High proliferation and a resulting high cell density were observed on the β-TCP scaffolds over the course of 3 weeks; the rMSCs had generated bridges between the pore-forming bars. Virtually all the pore space was occupied by cells. In addition, analysis of cell surface markers suggested that the phenotype did not alter during culture time.

There has been a lively interest in determining the optimum material pore size and structure. On the whole, most studies agree with a pore diameter in the range of 100–1000 μm [44–46], the necessity of interconnected pores, and interconnections of more than approximately 50 μm [47] to allow for tissue ingrowth and formation. Bohner and Baumgart [48] found that a pore diameter in the range of 200–800 μm is optimal but that this optimum depends on the size and type of bone to be substituted. The herein presented data demonstrate that the pore size of 450–850 μm together with the high pore interconnectivity of the β-TCP scaffold were appropriate for *in vitro* cell cultures. However, the β-TCP scaffolds barely stimulated cells *in vivo*, as they did not induce a response in the blank groups. The repair induced by the seeded rMSCs was only evident in the groups P-MSC-O/N and P-MSC-3w after 12 weeks.

Bearing in mind that PDGF-BB is involved in the initial phase of the bone regeneration process [28], it was spread on the alginate film of AP-scaffolds for fast release. Despite its chemotactic and mitogenic properties, and despite our hypothesis stating that it may be applied as a substitute for the rMSCs, it did not lead to any improvement in the course of the experiment. The PDGF-BB induced repair was in the range of 15–20%, similar to that of most of the rMSC and blank groups. Among the groups treated with a single element, rMSCs, PDGF-BB, or BMP-2, only BMP-2 induced a significantly higher repair. The overall data may suggest a tendency for an increased response with the combinations of BMP-2 and rMSCs. Although differences were not statistically significant, a synergistic

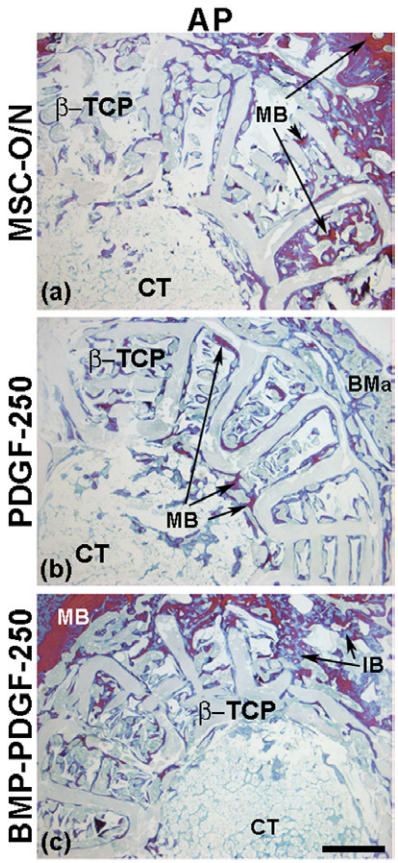

Figure 7. Representative photomicrographs of horizontal sections of calvaria defects in rats in the experimental groups AP-MSC-O/N (a), AP-PDGF-250 (b), and AP-BMP-PDGF-250 (c) confirming little defect repair at 4 weeks post-implantation. CT: connective tissue; β-TCP: beta-tricalcium phosphate; BMa: bone marrow; Ms: microspheres; IB: immature bone; MB: mineralized bone. Scale bar = 1 mm.

effect was observed after 12 weeks independent of the *in vitro* culture period and type of scaffold.

Also, PDGF-BB was included in the scaffold because of its indirect role in angiogenesis. Despite being more pronounced at short experimental periods, vascularization parameters tended to be higher in the PDGF-BB groups than in the BMP groups. Higher blood vessel densities were observed only in the groups treated with the combinations BMP-2 and MSCs or PDGF-BB (both doses) compared to single GF groups 12 weeks after implantation. The initial effect of PDGF-BB on new blood vessel formation and growth translates into vascular network restructuring and maturation in the long term. However, the effect observed at first decreased over the course of the 12 weeks, except for the BMP-2 groups. Thus, a greater amount of vascularized bone coincided with higher degree of repair. As a result of the poor bone formation in the non-BMP groups, these defects were partially filled with connective tissue with a reduced overall vascularization.

The modest bone repair observed in the groups treated with PDGF-BB alone was not unexpected and consistent with previous observations [49–51]. However, the expected synergistic effect when combining

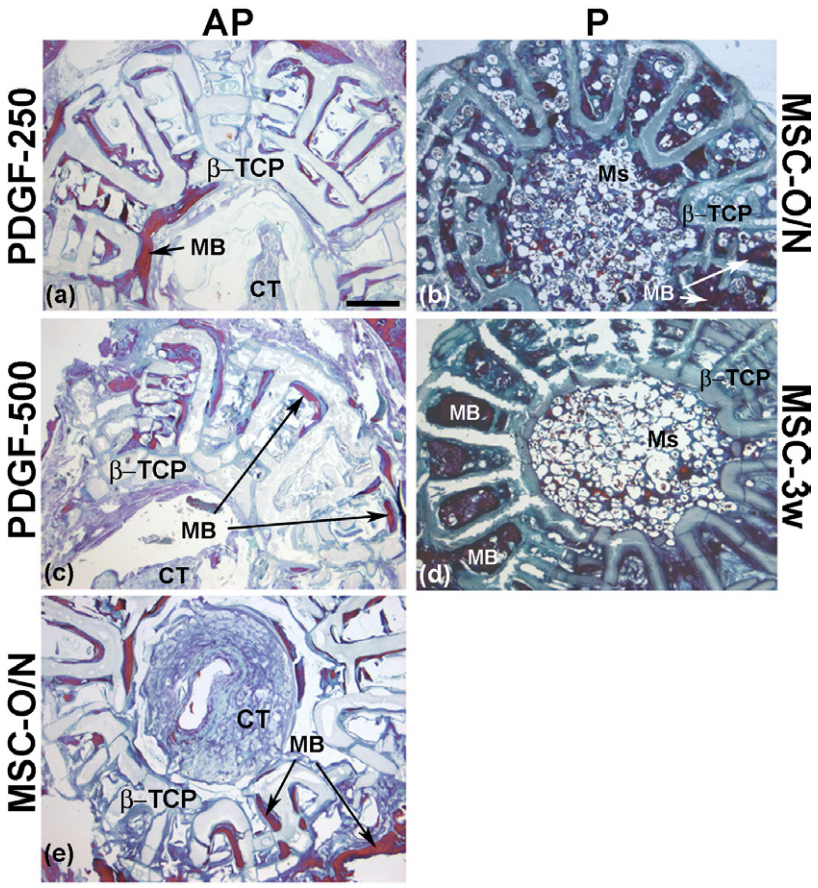

Figure 8. Representative photomicrographs of horizontal sections of calvaria defects in rat in the experimental groups AP-PDGF-250 (a), AP-PGDF-500 (c), AP-MSC-O/N (e), P-MSC-O/N (b), and P-MSC-3w (d) showing differential defect repair 8 weeks post-implantation. β-TCP: beta-tricalcium phosphate; CT: connective tissue; Ms: microspheres; MB: mineralized bone. Scale bar = 1 mm.

BMP and PDGF-BB was not observed. This combination even resulted in an antagonistic phenomenon—the bone-forming response with BMP-2 alone was higher than when combined with PDGF-BB. Despite its limitation, the literature about the effect of PDGF-BMP combinations is controversial. The different animal models, composition and architecture of scaffolds, and GF sources and the high doses used by some authors together with the fact that, to our knowledge, the literature does not reflect any study on the combination of PDGF-BB and BMP-2 with a scaffold prepared by robocasting all hinder direct comparison of our data. Zhang *et al* [52] reported that the delivery of PDGF-BB and BMP-7 encoding adenovirus through mesoporous bioglass/silk fibrin scaffolds induced significantly more new bone formations than the scaffolds alone or BMP-7-containing scaffolds in osteoporotic, critically sized femur defects in ovariectomized rats [52]. Park *et al* [53] observed that AdBMP2-transfected MSCs combined with 10 μg of PDGF-BB in a collagen hydrogel in an 8 mm, critically sized, calvarial defect led to high bone repair and significantly increased bone mineral density compared to the BMP-2/MSC group. Only Marden *et al* [54] observed an *in vivo* inhibitor effect of PDGF-BB on the bone regeneration induced by BMP-3 (osteogenin). The authors studied PDGF-BB in the dose range of 20–200 μg combined with 30 versus 150 μg of BMP-3 in an insoluble collagenous bone matrix implanted into 8 mm craniotomies in rats [54]. Similarly contradictory results were observed *in vitro*. Park *et al* [53] demonstrated *in vitro* that PDGF-BB suppresses osteogenic differentiation. The authors suggest attributing these findings to a reduced gene expression of BMP-2 [53]. Not only Park *et al* [53] but also Chan *et al* [55] observed the antagonistic effect of PDGF-BB on TGFβ family members. The authors showed that PDGF-BB induces microRNA-24, which downregulates Tribbles-like protein-3 (Trb3). Repression of Trb3 reduced expression of Smad proteins and consequently decreased BMP and TGFβ [55]. In contrast, the *in vitro* studies of Kim *et al* [56] revealed that the combination of PDGF-BB and BMP-2, immobilized in heparin functionalized titanium, enhanced osteoblast functions compared to the single GFs [56].

Part of these inconsistencies, found with the combinations of BMP-2 and PDGF, may have their origin in GF ratios, scaffold type, varying models for bone formation, and even assessment methods (i.e. x-ray opacity, micro-CT, bone mineral density versus histological analysis of bone area), which may be adding more confusion to the issue. Furthermore, it should be emphasized that all the previously cited studies lasted 4 weeks,

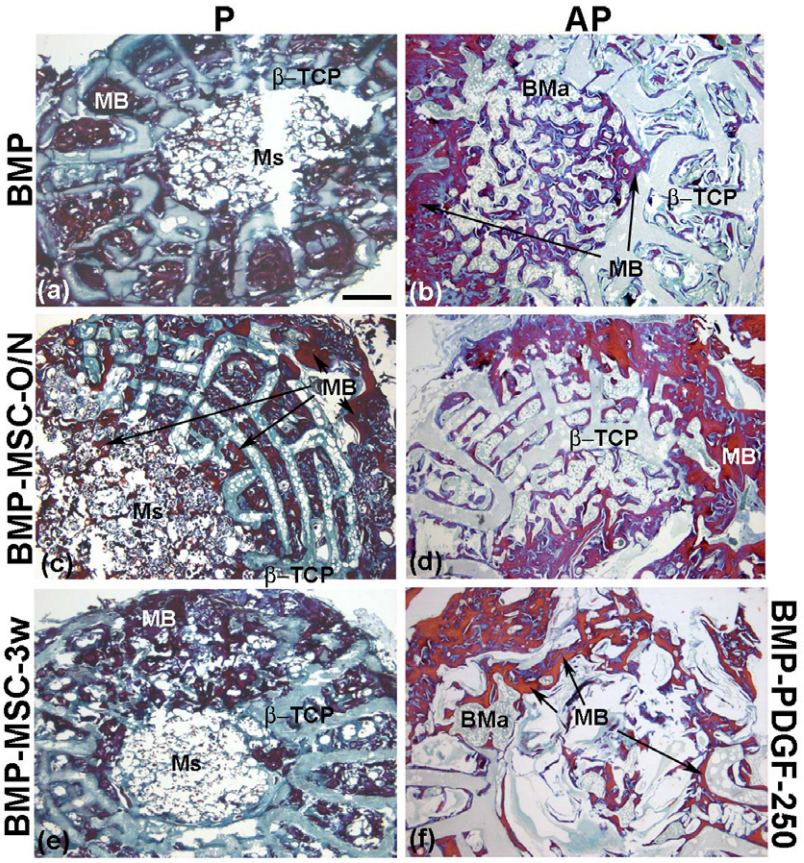

Figure 9. Representative photomicrographs of horizontal sections of calvaria defects in rats in the experimental groups P-BMP (a), AP-BMP (b), P-BMP-MSC-O/N (c), AP-BMP-MSC-O/N (d), P-BMP-MSC-3w (e), and AP-BMP-PDGF-250 (f) showing a high degree of defect repair with new bone formation in the β-TCP as well as in the central area of the scaffold 8 weeks post-implantation. β-TCP: beta-tricalcium phosphate; BMa: bone marrow; Ms: microspheres; MB: mineralized bone. Scale bar = 1 mm.

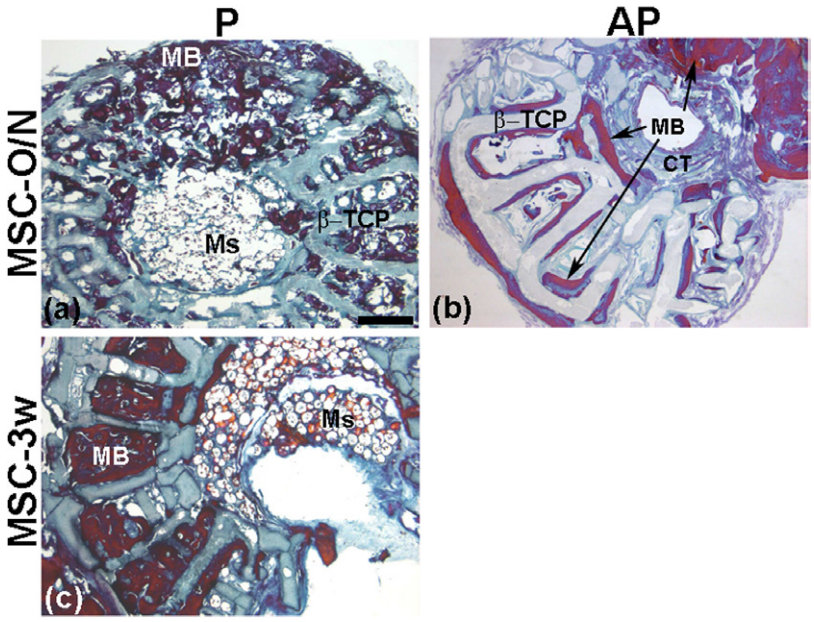

Figure 10. Representative photomicrographs of horizontal sections of calvaria defects in rats in experimental groups P-MSC-O/N (a), AP-MSC-O/N (b), and P-MSC-3w (c). Differential defect repair had occurred 12 weeks post-implantation in the β-TCP as well as the central area of the scaffold between the specimens implanted with either the P or the AP system. β-TCP: beta-tricalcium phosphate; CT: connective tissue; Ms: microspheres; MB: mineralized bone. Scale bar = 1 mm.

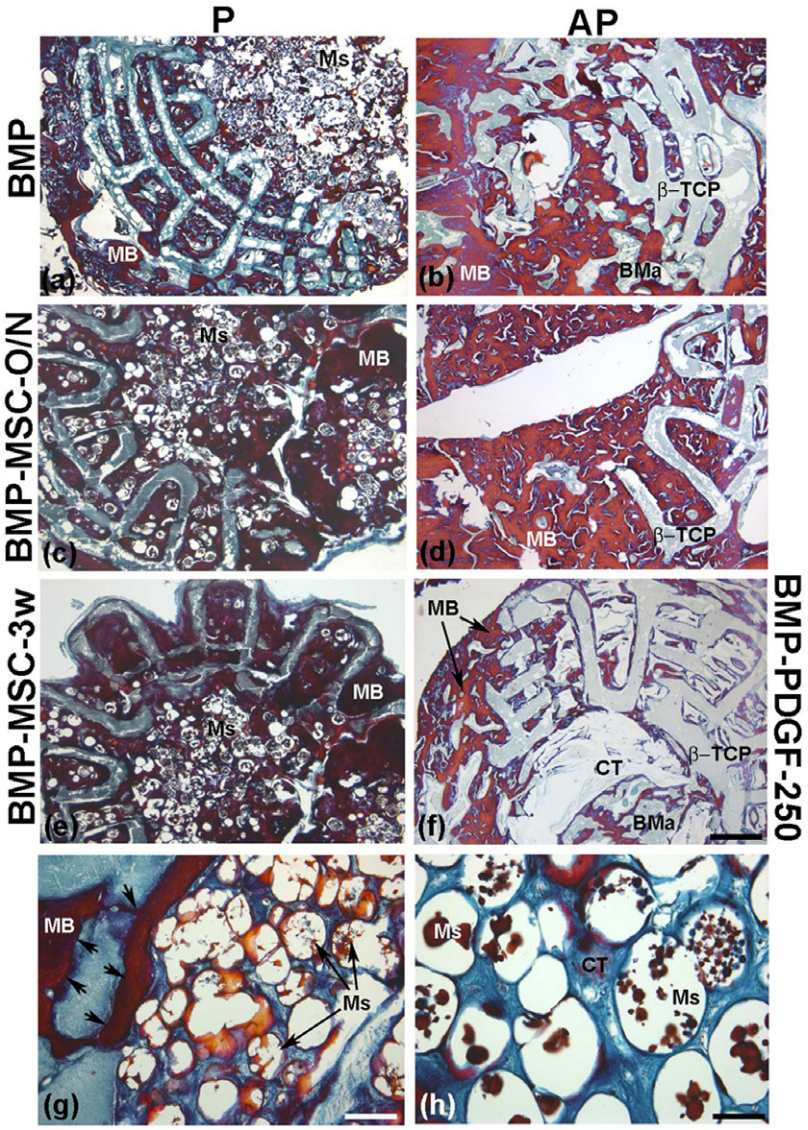

Figure 11. Representative photomicrographs of horizontal sections of calvaria defects in rats in the experimental groups P-BMP (a), AP-BMP (b), P-BMP-MSC-O/N (c), AP-BMP-MSC-O/N (d), P-BMP-MSC-3w (e), and AP-BMP-PDGF-250 (f) showing the highest degree of defect repair observed in all experimental groups 12 weeks post-implantation, except for group AP-BMP-PDGF-250. (g) Details at high magnification, illustrating newly formed bone in intimate contact with β-TCP (arrows) as well as residual PLGA 75:25 microspheres remaining at that moment. (h) High magnification photomicrograph of PLGA 50:50 microspheres immersed in connective tissue in the core of the system 4 weeks post-implantation. β-TCP: beta-tricalcium phosphate; BMa: bone marrow; Ms: microspheres; MB: mineralized bone. Scale bar = 1 mm (a-f), 250 μm (g), 100 μm (h).

whereas the inhibitory effect in this study was observed after 12 weeks. Also, the GF sources differed, such as GF encoding adenovirus, AdBMP2-transfected BMSCs, or recombinant GFs as presented in this study. Herein, the system was designed for a fast release of PDGF-BB to achieve a high PDGF/BMP ratio at an early stage. Hence, for the 250 ng of PDGF-BB combined with 6 μg of BMP-2, the ratio was, according to the release profiles, 10:1, 2:1, and 3:1, after 1, 4, and 7 d, respectively. However, most of the mentioned works did not study the *in vivo* GF release kinetics, with the exception of Marden *et al* [54]. Unfortunately, the latter work only provides the *in vivo* PDGF-BB release profile, which again does not contribute to data clarification. Moreover, the doses of PDGF-BB and BMP-2 used by other authors [53, 54] were 20-fold to 80-fold and 5-fold to 25-fold higher, respectively, than the doses used in this study. It is noteworthy that an increased dose of BMP-2 is not justified, at least in our system, because good repair can be induced with a smaller dose of a single GF. From an industrial-clinical point of view, even the slightly higher response obtained with the combinations of BMP-2 and rMSCs is not pronounced enough to accept the variability and complicate manipulation of cells compared to BMP-2 alone.

Finally, the BMP-2-containing RP scaffolds described in the literature differ in composition and architecture and even in defect size to be regenerated. Therefore, data cannot be compared easily. Specifically, RP scaffolds of poly ε-caprolactone/tricalcium phosphate/collagen [57] with 5 μg of BMP-2 and others made of bioactive glass [58] with 1 μg of BMP-2 were tested

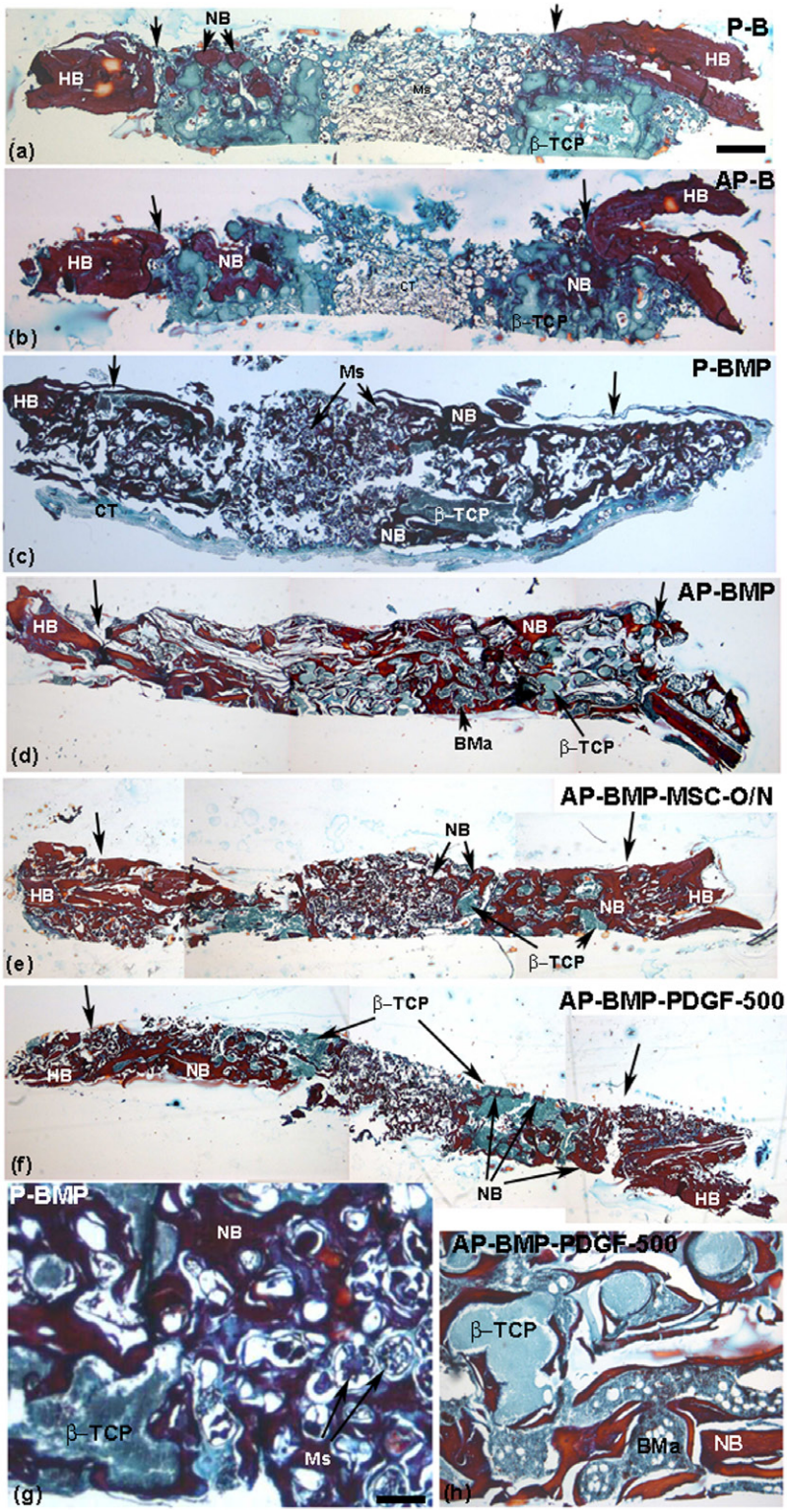

Figure 12. Representative photomicrographs of transversal sections of calvaria defects in rats from 12 weeks post-implantation in experimental groups P-B (a), AP-B (b), P-BMP (c), AP-BMP (d), AP-BMP-MSC-O/N (e), and AP-BMP-PDGF-500 (f) showing the characteristic structure of newly formed bone and its differential thickness between the groups implanted with the P and the AP systems. (g), (h) High-magnification details of the newly formed bone completely integrated into the scaffold structure. β-TCP fragments and PLGA 75:25 microspheres immersed in bone can be clearly observed in the group P-BMP (g). The equivalent image from group AP-BMP-PDGF-500 (h) does not reveal any more PLGA 50:50 microspheres, but reveals the presence of higher amounts of bone marrow instead. β-TCP: beta-tricalcium phosphate; BMa: bone marrow; CT: connective tissue; Ms: microspheres; HB: host bone; NB: new bone. Scale bar = 1 mm (a)–(f), 180 μm (g), (h).

with rat calvarial defects of 5 mm and 4.6 mm, respectively. Accordingly, those defects were smaller than the one created in this work, which was more challenging to regenerate. Thus, defects of a size like the aforementioned ones would have healed within 12 weeks after implantation of the robocast β-TCP scaffold.

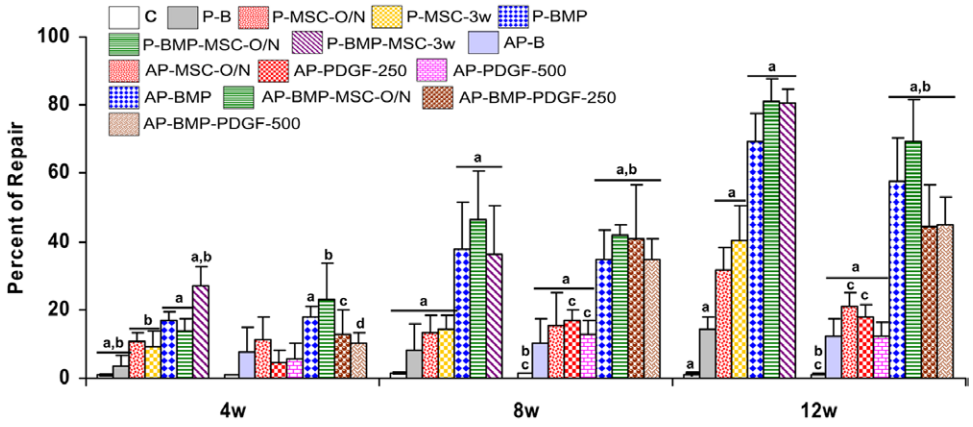

Figure 13. Histomorphometrical analysis. Comparison of the degrees of repair (%) between the two groups of scaffolds (P and AP) at different experimental time points ($n = 3$). The identical letter on different histograms indicates significant differences, $p < 0.05$.

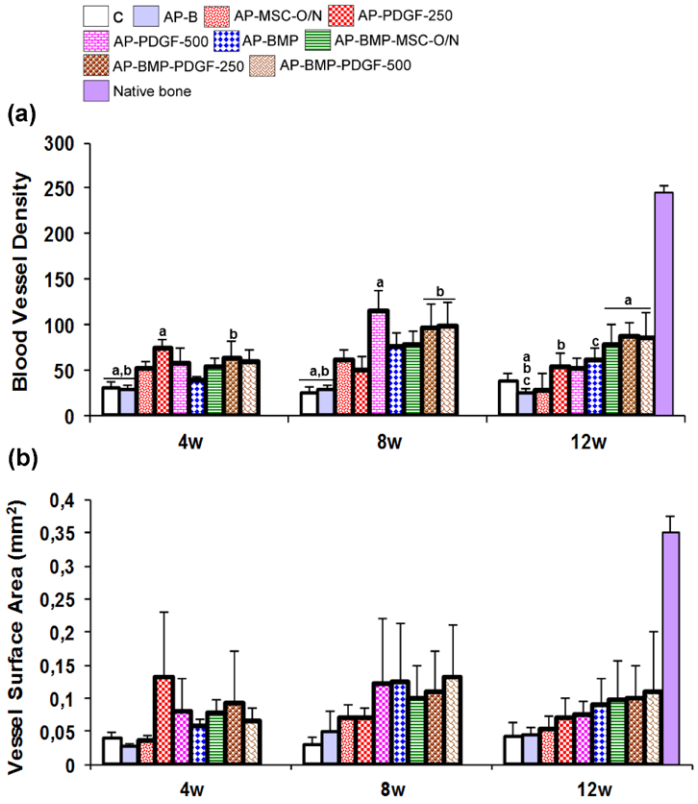

Figure 14. Bar graph representing blood vessel density (a) and vessel surface area (b) at different time points of analysis of the AP system. The identical letter on different histograms indicates significant differences, $p < 0.05$.

5. Conclusions

In conclusion, the porous β-TCP scaffolds used in this study resulted in a good cell viability and *in vivo* biocompatibility for bone regeneration. The generally observed lack of beneficial effect of the combined delivery of PDGF-BB and BMP-2 over BMP-2 alone could be result of a non-optimized dose ratio, release kinetics of GFs from the currently explored systems, or both. However, the increased response induced by adding BMP-2 to the rMSCs seeded scaffolds was not sufficient to justify the use of cells. Therefore, according to the high regeneration rate induced by BMP-2, it is not worthwhile combining BMP-2 with PDGF-BB or MSCs, at least with the herein proposed porous scaffold and defect model.

Financial disclosure

The authors declare no competing financial interest.

Acknowledgments

This work was supported by the Ministry of Science and Technology (MAT2011-23819 to CÉ) and Proyecto Motiva of ACIISI. MR-É was supported by *Beca*

CajaCanarias para posgraduados. The authors thank the members of the Department of Cell Biology of the University of La Laguna for receiving RR in their laboratory. The authors thank Dr Carmen Damas for assistance with statistical analysis.

References

[1] Damien C J and Parsons J R 1991 Bone graft and bone graft substitutes: a review of current technology and applications *J. Appl. Biomater.* **2** 187–208

[2] Mankin H J and Gebhardt M C 1996 Long term results of allograft replacement in the management of bone tumours *Clin. Orthop. Relat. Res.* **324** 86–97

[3] Simonds R J *et al* 1992 Transmission of human immunodeficiency virus type 1 from a sero-negative organ and tissue donor *N. Engl. J. Med.* **326** 726–32

[4] Kasten P, Beyen I, Niemeyer P, Luginbühl R, Bohner M and Richter W 2008 Porosity and pore size of β-tricalcium phosphate scaffold can influence protein production and osteogenic differentiation of human mesenchymal stem cells: an *in vitro* and *in vivo* study *Acta Biomater.* **4** 1904–15

[5] Kee-Won L, Shanfeng W, Mahrokh D, Yaszemski M J and Lu L 2010 enhanced cell ingrowth and proliferation through 3D nanocomposite scaffolds with controlled pore structures *Biomacromolecules* **11** 682–9

[6] Kyobum K, Dean D, Wallace J, Breithaupt R, Mikos A G and Fisher J P 2011 The influence of stereolithographic scaffold architecture and composition on osteogenic signal expression with rat bone marrow stromal cells *Biomaterials* **32** 3750–63

[7] Gil-Albarova J, Vila M, Badiola-Vargas J, Sánchez-Salcedo S, Herrera A and Vallet-Regi M 2012 *In vivo* osteointegration of 3D crosslinked gelatin-coated hydroxyapatite foams *Acta Biomater.* **8** 3777–83

[8] Rodríguez-Évora M, Delgado A, Reyes R, Hernández-Daranas A, Soriano I, San Román J and Évora C 2013 Osteogenic effect of local, long versus short term BMP-2 delivery from a novel SPU-PLGA-βTCP concentric system in a critical size defect in rats *Eur. J. Pharm. Sci.* **49** 873–84

[9] Cao H and Kuboy N 2010 A biodegradable porous composite scaffold of PGA/β-TCP for bone tissue engineering *Bone* **46** 386–95

[10] Sun F, Zhou H and Lee J 2011 Various preparation methods of highly porous hydroxyapatite/polymer nanoscale biocomposites for bone regeneration *Acta Biomater.* **7** 3813–28

[11] Sanzana E S, Navarro M, Ginebra M P, Planell J A, Ojeda A C and Montecinos H A 2013 Role of porosity and pore architecture in the *in vivo* bone regeneration capacity of biodegradable glass scaffolds *J. Biomed. Mater. Res.* A **102** 1767–73

[12] Hutmacher D W 2000 Scaffolds in tissue engineering bone and cartilage *Biomaterials* **21** 2529–43

[13] Yeong W Y, Chua C K, Leong K F and Chandrasekaran M 2004 Rapid prototyping in tissue engineering: challenges and potencial *Trends Biotechnol.* **22** 643–52

[14] Butscher A, Bohner M, Hofmann S, Gauckler L and Müller R 2011 Structural and material approaches to bone tissue engineering in powder-based 3D printing *Acta Biomater.* **7** 907–20

[15] Hoque M E, Chuan Y L and Pashby I 2012 Extrusion based rapid prototyping technique: an advanced platform for tissue engineering scaffold fabrication *Biopolymers* **97** 83–93

[16] Serra T, Planell J A and Navarro M 2013 High-resolution PLA-based composite scaffolds via 3D printing technology *Acta Biomater.* **9** 5521–30

[17] Miranda P, Saiz E, Gryn K and Tomsia A P 2006 Sintering and robocasting of beta-tricalcium phosphate scaffolds for orthopaedic applications *Acta Biomater.* **2** 457–66

[18] Martinez-Vazquez F J, Perera F H, Miranda P, Pajares A and Guiberteau F 2010 Improving the compressive strength of bioceramic robocast scaffolds by polymer infiltration *Acta Biomater.* **6** 4361–68

[19] Richard R C, Sader M S, Dai J, Thire R M S M and Soares G D A 2014 Beta-type calcium phosphates with and without magnesium: from hydrolysis of brushite powder to robocasting of periodic scaffolds *J. Biomed. Mater. Res.* A **102A** 3685–92

[20] Franco J, Hunger P, Launey M E, Tomsia A P and Saiz E 2010 Direct write assembly of calcium phosphate scaffolds using a water-based hydrogel *Acta Biomater.* **6** 218–28

[21] Sánchez-Salcedo S, Nieto A and Vallet-Regí M 2008 Hydroxyapatite/β-tricalcium phosphate/agarose macroporous scaffolds for bone tissue engineering *Chem. Eng. J.* **137** 62–71

[22] Levengood S K L, Polak S J, Wheeler M B, Maki A J, Clark S G, Jamison R D and Wagoner Jonhson A J 2010 Multiscale osteointegration as a new paradigm for the design of calcium phosphate scaffolds for bone regeneration *Biomaterials* **31** 3552–63

[23] Lacefield W R 1993 Hydroxylapatite coatings *An Introduction to Bioceramics* ed L L Hench (Singapore: World Scientific) p 223

[24] Liu B and Lun D X 2012 Current application of β-tricalcium phosphate composites in orthopaedics *Orthop. Surg.* **4** 139–44

[25] Akiyama K, You Y O, Yamaza T, Chen C, Tang L, Jin Y, Chen X D, Gronthos S and Shi S 2012 Characterization of bone marrow derived mesenchymal stem cells in suspension *Stem Cell Res. Ther.* **3** 40

[26] Devescovi V, Leonardi E, Ciapetti G and Cenni E 2008 Growth factors in bone repair *Chir. Organi. Mov.* **92** 161–8

[27] Hollinger J O, Hart C E, Hirsch S N, Lynch S and Friedlaender G E 2008 Recombinant human platelet-derived growth factor: biology and clinical applications *J. Bone Joint Surg. Am.* **90** 48–54

[28] Dimitriou R, Tsiridis E and Giannoudis P V 2005 Current concepts of molecular aspects of bone healing *Injury* **36** 1392–1404

[29] Lee K, Silva E A and Mooney D J 2011 Growth factor delivery-based tissue engineering: general approaches and a review of recent developments *J. R. Soc. Interface* **8** 153–70

[30] Kanczler J M and Oreffo R O 2008 Osteogenesis and angiogenesis: the potencial for engineering bone *Eur. Cell Mater.* **15** 100–14

[31] Miranda P, Pajares A, Saiz E, Tomsia A P and Guiberteau F 2008 Mechanical properties of calcium phosphate scaffolds fabricated by robocasting *J. Biomed. Mater. Res.* A **85A** 218–27

[32] Martinez-Vazquez F J, Perera F H, van der Meulen I, Heise A, Pajares A and Miranda P 2013 Impregnation of β-tricalcium phosphate robocast scaffolds by *in situ* polymerization *J. Biomed. Mater. Res.* A **101** 3086–96

[33] Hernández A, Sánchez E, Soriano I, Reyes R, Delgado A and Évora C 2012 Material-related effects of BMP-2 delivery systems on bone regeneration *Acta Biomater.* **8** 781–91

[34] Fraker P J and Speck J C Jr 1978 Protein and cell membrane iodinations with a sparingly soluble chloroamide, 1,3,4,6-tetrachloro-3a,6a-diphrenylglycoluril *Biochem. Biophys. Res. Commun.* **80** 849–57

[35] De la Riva B, Nowak C, Sánchez E, Hernández A, Schulz-Siegmund M, Pec M K, Delgado A and Evora C 2009 VEGF-controlled release within a bone defect from alginate/chitosan/PLA-H scaffolds *Eur. J. Pharm. Biopharm.* **73** 50–8

[36] Dobson K R, Reading L, Haberey M, Marine X and Scutt A 1999 Centrifugal isolation of bone marrow from bone: an improved method for the recovery and quantitation of bone marrow osteoprogenitor cells from rat tibiae and femurae *Calcif. Tissue Int.* **65** 411–3

[37] Spicer P P, Kretlow J D, Young S, Jansen J A, Kasper F K and Mikos A G 2012 Evaluation of bone regeneration using the rat critical size calvarial defect *Nat. Protoc.* **7** 1918–29

[38] Delgado J J, Évora C, Sánchez E, Baro M and Delgado A 2006 Validation of a method for non-invasive *in vivo* measurement of growth factor release from a local delivery system in bone *J. Control. Release* **114** 223–9

[39] Hernández A, Reyes R, Sánchez E, Rodríguez-Évora M, Delgado A and Évora C 2012 *In vivo* osteogenic response to different ratios of BMP-2 and VEGF released from a biodegradable porous system *J. Biomed. Mater. Res.* A **100** 2382–91

[40] Martínez-Sanz E, Ossipov D A, Hilborn J, Larsson S, Jonsson K B and Varghese O P 2011 Bone reservoir: injectable hyaluronic acid hydrogel for minimal invasive bone augmentation *J. Control. Release* **152** 232–40
[41] Boxall SA and Jones E 2012 Markers for characterization of bone marrow multipotential stromal cells *Stem Cells Int.* **2012** 975871
[42] Bidan C M, Kommareddy K P, Rumpler M, Kollmannsberger P, Fratzl P and Dunlop J W 2013 Geometry a as factor for tissue growth: towards shape optimization of tissue engineering scaffolds *Adv. Healthcare Mater.* **2** 186–94
[43] McMurray R J, Gadegaard N, Tsimbouri P M, Burgess K V, McNamara L E, Tare R, Murawski K, Kingham E, Oreffo R O C and Dalby M J 2011 Nanoscale surfaces for the long-term maintenance of mesenchymal stem cell phenotype and multipotency *Nat. Mater.* **10** 637–44
[44] Uchida A, Nade S M, McCartney E R and Ching W 1984 The use of ceramics for bone replacement. A comparative study of three different porous ceramics *J. Bone Joint Surg. Br.* **66** 269–75
[45] Chang B S, Lee C K, Hong K S, Youn H J, Ryu H S, Chung S S and Park K W 2000 Osteoconduction at porous hydroxyapatite with various pore configurations *Biomaterials* **21** 1291–98
[46] Chu T M, Orton D G, Hollister S J, Feinberg S E and Halloran J W 2002 Mechanical and *in vivo* performance of hydroxyapatite implants with controlled architectures *Biomaterials* **23** 1283–93
[47] Lu J X, Flautre B, Anselme K, Hardouin P, Gallur A, Descamps M and Thierry B 1999 Role of interconnections in porous bioceramics on bone recolonization *in vitro* and *in vivo* *J. Mater. Sci. Mater. Med.* **10** 111–20
[48] Bohner M and Baumgart F 2004 Theoretical model to determine the effects of geometrical factors on the resorption of calcium phosphate bone substitutes *Biomaterials* **25** 3569–82
[49] De la Riva B, Sánchez E, Hernández A, Reyes R, Tamimi F, López-Cabarcos E, Delgado A and Évora C 2010 Local controlled release of VEGF and PDGF from a combined brushite–chitosan system enhances bone regeneration *J. Control. Release* **143** 45–52
[50] Delgado J J, Sánchez E, Baro M, Reyes R, Évora C and Delgado A 2012 A platelet derived growth factor delivery system for bone regeneration *J. Mater.Sci. Mater. Med.* **23** 1903–12
[51] Kaipel M, Schützenberger S, Schultz A, Ferguson J, Slezak P, Morton T J, Van Griensven M and Redl H 2012 BMP-2 but not VEGF or PDGF in fibrin matrix supports bone healing in a delayed-union rat model *J. Orthop. Res.* **30** 1563–69
[52] Zhang Y, Cheng N, Miron R, Shi B and Cheng X 2012 Delivery of PDGF-B and BMP-7 by mesoporous bioglass/silk fibrin scaffolds for the repair of osteoporotic defects *Biomaterials* **33** 6698–708
[53] Park S Y, Kim K H, Shin S Y, Koo K T, Lee Y M and Seol Y J 2013 Dual delivery of rhPDGF-BB and bone marrow mesenchymal stromal cells expressing the BMP2 gene enhance bone formation in a critical-sized defect model *Tissue Eng.* A **19** 2495–505
[54] Marden L J, Fan R S, Pierce G F, Reddi A H and Hollinger J O 1993 Platelet-derived growth factor inhibits bone regeneration induced by osteogenin, a bone morphogenetic protein, in rat craniotomy defects *Clin. Invest.* **92** 2897–905
[55] Chan M C, Hilyard A C, Wu C, Davis B N, Hill N S, Lal A, Lieberman J, Lagna G and Hata A 2010 Molecular basis for antagonism between PDGF and the TGFβ family of signalling pathways by control of miR-24 expression *EMBO J.* **29** 559–73
[56] Kim S E, Yun Y P, Lee J Y, Shim J S, Park K and Huh J B 2013 Co-delivery of platelet-derived growth factor (PDGF-BB) and bone morphogenic protein (BMP-2) coated onto heparinized titanium for improving osteoblast function and osteointegration *J. Tissue Eng. Regen. Med.* doi:10.1002/term.1668
[57] Sawyer A A, Song S J, Susanto E, Chuan P, Lam C X F, Woodruff M A, Hutmacher D W and Cool S M 2009 The stimulation of healing within a rat calvarial defect by mPCL–TCP/collagen scaffolds loaded with rhBMP-2 *Biomaterials* **30** 2479–88
[58] Liu X, Rahaman M N, Liu Y, Bal B S and Bonewald L F 2013 Enhanced bone regeneration in rat calvarial defects implanted with surface-modified and BMP-loaded bioactive glass (13–93) scaffolds *Acta Biomater.* **9** 7506–17